

#### **PAPER**

# Mobility of nano-sized ½(111) vacancy and interstitial prismatic dislocation loops in tungsten

To cite this article: Jan Fikar et al 2025 Modelling Simul. Mater. Sci. Eng. 33 065006

View the article online for updates and enhancements.

# You may also like

- Deterministic equivalent and error universality of deep random features learning
   Dominik Schröder Hugo Cui Daniil
- Dominik Schröder, Hugo Cui, Daniil Dmitriev et al.
- Quantum computer-enabled receivers for optical communication
   John Crossman, Spencer Dimitroff, Lukasz Cincin et al.
- High-dimensional robust regression under heavy-tailed data: asymptotics and universality

Urte Adomaityte, Leonardo Defilippis, Bruno Loureiro et al.

# Mobility of nano-sized $1/2\langle 1\,1\,1\rangle$ vacancy and interstitial prismatic dislocation loops in tungsten

Jan Fikar<sup>1,\*</sup>, Robin Schäublin<sup>2</sup>, Daniel R Mason<sup>3</sup> and Duc Nguyen-Manh<sup>3</sup>

- <sup>1</sup> Institute of Physics of Materials, The Czech Academy of Sciences, Žižkova 22, 616 00 Brno, Czech Republic
- <sup>2</sup> Laboratory of Metal Physics and Technology, Department of Materials, ETH Zürich, 8093 Zürich, Switzerland
- <sup>3</sup> CCFE, Culham Campus, Abingdon, OX14 3DB Oxfordshire, United Kingdom

E-mail: fikar@ipm.cz

Received 27 February 2025; revised 7 July 2025 Accepted for publication 15 July 2025 Published 1 August 2025



#### **Abstract**

The vacancies and interstitials produced in high-energy collision cascades of irradiated tungsten can form prismatic dislocation loops with Burgers vectors  $^{1}/_{2}\langle 1\,1\,1\rangle$  and  $\langle 1\,0\,0\rangle$ . The  $^{1}/_{2}\langle 1\,1\,1\rangle$  loops are very mobile, and their mobility is essential for the microstructure development of irradiated materials, It is a key parameter for predictive models such as kinetic Monte Carlo. We investigated the mobility of  $^{1}/_{2}\langle 1\,1\,1\rangle$  vacancy and interstitial hexagonal loops as a function of their size using the recent embedded-atom method tungsten potential. The phonon drag phenomenon occurs at high temperatures and can be separated during post-processing from the thermally activated motion. The magnitude of the phonon drag at 300 K was evaluated and appeared to be critical for single interstitial atoms, with a nearly ten-fold increase of their diffusion, while dislocation loops are less influenced.

Keywords: prismatic dislocation loop, radiation damage, molecular dynamics, mean square displacement, tungsten, diffusion

#### 1. Introduction

Tungsten is a leading candidate material for plasma-facing components in future fusion reactors, valued for its high melting point and resistance to sputtering. However, under operational conditions, its microstructure will be constantly subjected to high-energy particle irradiation,

© 2025 IOP Publishing Ltd.

<sup>\*</sup> Author to whom any correspondence should be addressed.

which generates a variety of lattice defects that can degrade its mechanical properties. Recent experimental [1, 2] and computational [3, 4] studies have shown that these defects are nanoscale prismatic dislocation loops formed directly within displacement cascades.

In tungsten, transmission electron microscope (TEM) observations [5, 6] reveal that these prismatic loops have Burgers vectors of  $^1/_2\langle 111\rangle$  and  $\langle 100\rangle$ . The  $^1/_2\langle 111\rangle$  loops are highly mobile, whereas the  $\langle 100\rangle$  loops are mobile only at very high temperatures [7]. In the following, we focus on highly mobile  $^1/_2\langle 111\rangle$  loops in tungsten.

The parameters of thermally activated mobility of the loops are important in predicting the development of the irradiated materials at larger time scales using kinetic Monte Carlo methods. The parameters are usually obtained by several long isothermal molecular dynamics (MD) simulations, where the position of the loop is recorded as a function of the elapsed time. Then, its trajectory is analyzed, and the mean square displacement (MSD) is calculated, which can be related to the diffusivity D using the Einstein diffusion equation,

$$D = \frac{\left\langle \left(r - r_0\right)^2 \right\rangle}{2nt},\tag{1}$$

where n is the dimensionality of the movement and t is time. The diffusivity itself is usually thermally activated and obeys the Arrhenius law,

$$D = D_0 \exp\left(\frac{-E_{\text{mig}}}{kT}\right),\tag{2}$$

where  $E_{\text{mig}}$  is the migration energy and  $D_0$  is the diffusivity at infinite temperature. The parameter  $D_0$  corresponds to the situation where the probability of jumping equals one, so the loop will jump to the new position during every attempt,

$$D_0 = b^2 \nu, \tag{3}$$

where b is the Burgers vector and  $\nu$  is the attempt frequency, sometimes for point defects approximated by Debye frequency.

MSD and diffusivity D obtained for different temperatures T allow us to fit the Arrhenius equation (2) and obtain the two parameters for thermally activated motion  $E_{\text{mig}}$  and  $D_0$ .

Alternatively,  $E_{\text{mig}}$  can be determined as the energy barrier height using the nudged elastic band (NEB) method [8]. However, NEB does not provide  $D_0$ .

Two limitations of the MSD method for single interstitial atom (SIA) diffusion in tungsten were discovered recently. First, the diffusivity of an SIA in tungsten above 150 K is linear with temperature and does not follow Arrhenius law. This effect is explained by Swinburne *et al* as a phonon drag phenomenon [9]. Second, the diffusivity at low temperatures is influenced by quantum zero vibrations, and in tungsten, it already appears below 100 K [10]. MSD cannot be efficiently used, as there is not a large enough temperature window to fit the Arrhenius law.

The low-temperature quantum effects are not a problem for classical MSD calculations. The diffusivity calculated by classical MD at low temperatures can be used to fit the Arrhenius parameters  $D_0$  and  $E_{\rm mig}$ . On the contrary, equation (2) should not be used to determine the real loop mobility at low temperatures  $D(T < 100 \, {\rm K})$ .

The high-temperature phonon drag is also sometimes explained as a correlation of SIA jumps. In the case of 1D diffusion, the correlation factor f is a ratio of the number of jumps forward and backward relative to the direction of the previous jump. Zhou *et al* found by MD that the correlation factor for SIA diffusion in tungsten is 2.77-2.44 for temperatures 300-900 K [11]. We think that there is no microscopical reason why, in the case of 1D SIA diffusion, the jump should depend on the direction of the previous jump, and thus, in our

opinion, f should be equal to 1. We think the observed f > 1 can be explained as jumps longer than one Burgers vector, which are then interpreted as several jumps in the same direction.

We will show how to separate the long jumps by post-processing the MSD data effectively. The objective of this paper is to calculate the parameters of thermally activated diffusivity of the  $^{1}/_{2}\langle 1\,1\,1\rangle$  prismatic loops and compare it with diffusivity, including phonon drag phenomenon, also sometimes called correlated diffusion.

### 2. Computational details

The procedure for creating the sample with the dislocation loops is described in our previous paper [12]. We investigated perfect hexagonal  $^1/_2\langle 1\,1\,1\rangle$  loops containing 1, 19, 61, 127, 217, and 397 defects. The hexagonal shape was chosen because it has the lowest formation energy and the highest mobility in tungsten [7]. The largest loop has a diameter of 5.5 nm. Since the dislocation loop creates a long-range deformation field, the simulation block should be at least four times larger than the loop diameter [13]. For the largest loop with 397 defects, the simulation block contains approximately 1.6 million atoms, corresponding to a simulation box side length of 29 nm. The smallest simulation block for single defects and 19-defects loops has 19 thousand atoms and has box side of 7 nm. The nearly cubic simulation boxes with periodic boundary conditions are oriented in directions  $\langle \bar{1}\,1\,0\rangle$ ,  $\langle 1\,1\,1\rangle$ , and  $\langle 1\,1\,\bar{2}\rangle$  with the Burgers vector aligned along the *y*-axis.

The simulation block is first relaxed using the conjugate gradient (CG) method in LAMMPS [14]. It then isothermally evolves for a long time at a specific temperature range of 25–800 K. We use the NPT ensemble to accommodate thermal expansion. The long MD simulations tend to accumulate a certain drift due to numerical errors. In our simulations the drift is avoided by periodically zeroing the total momentum of all atoms each 1000 MD steps. Typically, there is a problem detecting the exact loop position at higher temperatures due to the thermal noise. We use MD with an integration time step of  $\Delta t$  of 2 fs and integrate for  $1000\Delta t$ , i.e. 2 ps, which we call a step. After each step, a restart file is written, from which the simulation can continue seamlessly. Then, a CG is applied to find the precise loop position. The loop is detected using common neighbor analysis (CNA). The average position of the atoms with CNA different from perfect BCC gives the center of the loop. The covariance matrix of the positions of these CNA-detected atoms is also recorded, as its large eigenvalues are a good indication of the loop crossing periodic boundaries. Then, the isothermal MD is continued from the restart file, which results in an uninterrupted simulation. In total we simulate 5000 such steps, corresponding to 10 ns.

A typical result can be seen in figure 1, where the absolute value of the difference in position of the loop  $|\Delta y|$  in each step is shown. At low temperatures, we observe only jumps up to one Burgers vector i.e. 1b, while at higher temperatures around 150–200 K longer jumps start to appear, and their number increases with temperature. The jumps up to 1b are thus considered thermally activated, i.e. Arrhenius behavior, while larger jumps represent the phonon drag phenomenon, also sometimes called correlated diffusion.

Now, we can use all the points, which will give us the total diffusivity, including the phonon drag phenomenon. Alternatively, we can discard all the jumps larger than 1b and calculate thermally activated diffusivity, which can then be used in the Arrhenius fit by equation (2). Typically, ten different temperatures in the 25–800 K range are fitted for each loop. Lower temperatures are employed for highly mobile defects, while higher temperatures are used for less mobile defects. It could, in principle, happen that during step two, independent thermally activated jumps occur in the same direction, which will be during our post-processing incorrectly interpreted as phonon drag. Our chosen step of 2 ps is a compromise, approximately

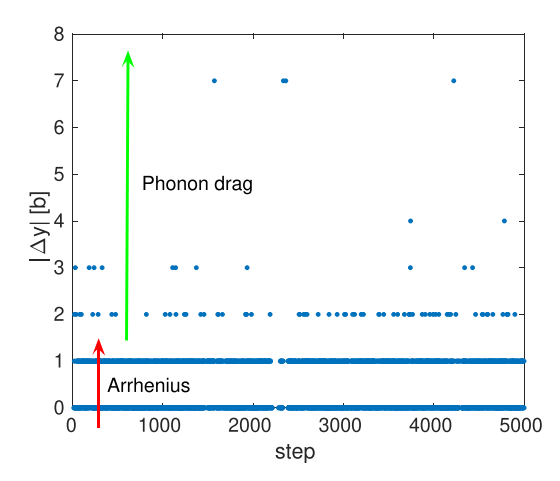


**Figure 1.** The absolute value of the difference in y position parallel to the Burgers vector of the 127 vacancy loop at 800 K in each step. The jumps up to 1b are considered thermally activated, i.e. Arrhenius, larger jumps represent the phonon drag phenomenon sometimes called the correlated diffusion.

ten Debye periods long. Shorter steps will decrease the risk of detecting a long jump instead of two short jumps, but it will increase the calculation time, as more CG steps per the same amount of MD steps will be needed.

In our MD simulations, we use the recent embedded atom model (EAM) potential of Mason, Nguyen-Manh, and Becquart (*MNB*) [15], which is an enhancement of Ackland–Thetford *AT* potential [16] mainly in the better description of vacancy clusters.

### 3. Results and discussion

Almost all the loops undergo 1D random motion in the direction of their Burgers vector. There are three exceptions: the single vacancy moves in 3D and with much higher activation energy (see table 3). The SIA exhibits 1D movement up to a temperature of 500 K. Above this temperature, it can change direction, resulting in 3D movement. In this study, we focused solely on the one-dimensional movement of the SIA. The 19 vacancy loop does not move up to 800 K, but at 800 K, its formation energy is gradually decreasing. We conclude that the 19 vacancy loop is at 800 K transforming into a 19 vacancy void, which has lower formation energy, as we discovered in our previous paper [12]. All the vacancy loops up to 50 thousand voids (diameter of 65 nm) will probably transform into energetically favorable voids at sufficiently high temperatures and long times.

The thermal activation parameters as a function of the number of defects N are reported in figure 2. The migration energy  $E_{\rm mig}$  of the vacancy loops is decreasing with N, while it stays low all the time for interstitial loops. The diffusivity at infinite temperature  $D_0$  seems to be correlated with  $E_{\rm mig}$ . For example, lower  $E_{\rm mig}$  for 127 interstitial loop is somehow compensated by lower  $D_0$ . This correlation seems to be well fitted by the Meyer–Neldel (MN) enthalpy-entropy compensation rule [17, 18]

$$D_0 = D_{00} e^{E_{\text{mig}}/\Delta_{MN}},\tag{4}$$

where  $D_{00}$  and  $\Delta_{MN}$  are constants, the latter is called the MN barrier. The MN rule fit can be seen in figure 3; the resulting MN barriers  $\Delta_{MN}$  are  $10\pm3$  meV and  $22\pm3$  meV for interstitial and vacancy loops, respectively.

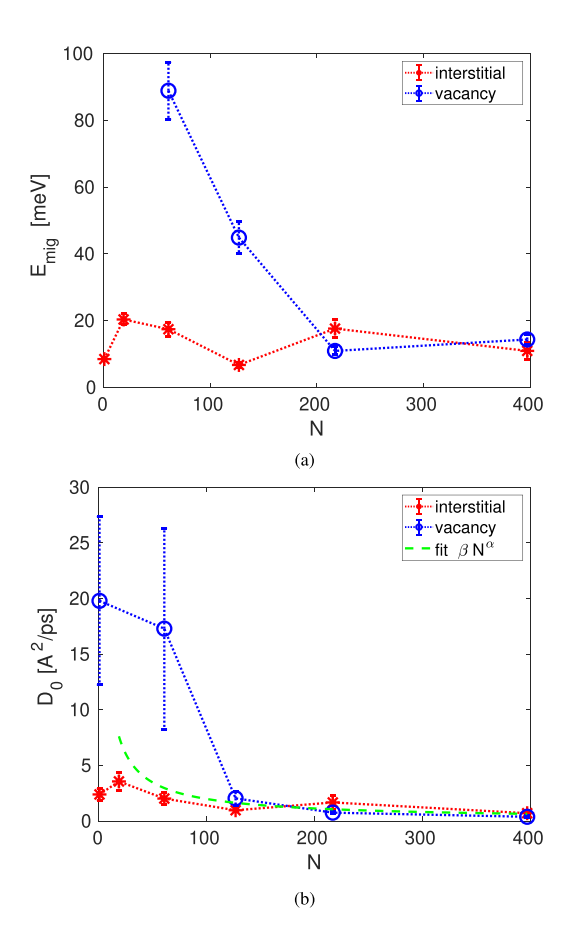


**Figure 2.** The loop thermally activated mobility parameters obtained by Arrhenius fit as a function of the number of defects N. The error bars correspond to standard deviations. (a)  $E_{\rm mig}$  migration energy (note one single vacancy moves in 3D and has an activation energy of 1050 meV). (b)  $D_0$  diffusivity at infinite temperature. Fitted  $\alpha = -0.81 \pm 0.29$ ,  $\beta = 4.4 \pm 1.4 \, {\rm Å}^2 \, {\rm ps}^{-1}$ .

The migration energy of 130 meV for 55 vacancy loop in tungsten was previously reported by Mason *et al* [5], which agrees well with our values. Becquart *et al* [19] reported for interstitial loops and SIA in tungsten migration energy of 13 meV and  $D_0$  of  $45N^{-1/2}$  Å<sup>2</sup> ps<sup>-1</sup>. These values are often used in Monte-Carlo simulations. While the migration energy agrees well with our results, our  $D_0$  is about three times smaller for loops and 19 times smaller for SIA. Derlet *et al* reported a similar migration energy of 39.6 meV and  $D_0$  of 1.19 Å<sup>2</sup> ps<sup>-1</sup> for 61 vacancy loop in BCC iron [20].

Chen *et al* reported migration energies and attempt frequencies for SIA and loops consisting of 7–85 interstitials using own Y-C\_2 tungsten potential described in the same paper [21]. The values are summarized in table 2. While the  $D_0$  is similar to our values, except for the SIA, the migration energies are higher than our values. It is either caused by difference in the interatomic potentials, or they are higher because the correlated diffusion was not taken into account. Fang *et al* reported diffusivity at 300 K of 19, 55 and 109 interstitial  $\frac{1}{2}(111)$  loops in tungsten using the same Y-C\_2 potential [22]. They are 0.52, 0.33 and 0.13 Å<sup>2</sup> ps<sup>-1</sup>, respectively. Our diffusivity for comparable loops at 300 K are slightly higher. The diffusivity at 300 K obtained from the thermal activation parameters of the Y-C\_2 potential 2 are 1.21,

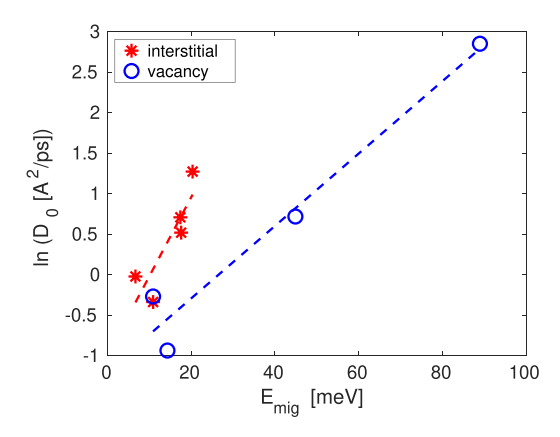


**Figure 3.** Meyer–Neldel enthalpy-entropy compensation rule for the activation parameters of the loop diffusion. The fitted MN barriers  $\Delta_{MN}$  are  $10\pm3$  meV and  $22\pm3$  meV for interstitial and vacancy loops, respectively.

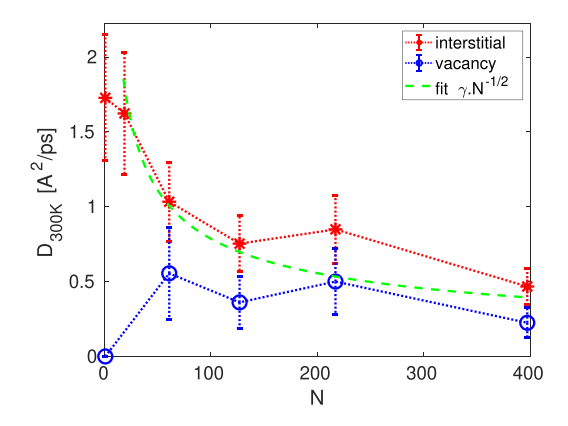


**Figure 4.** The thermally activated diffusivity of vacancy and interstitial loops at 300 K. The error bars correspond to standard deviations. The interstitial loop diffusivity fitted by  $N^{-1/2}$  [20],  $\gamma = 7.9 \pm 1.6 \,\text{Å}^2 \,\text{ps}^{-1}$ .

0.84, and 0.65  $\text{Å}^2 \, \text{ps}^{-1}$  for close sizes 19, 61, and 85, respectively. This is also higher than the values reported by Fang *et al*. The difference may be explained due to the presence of the free surfaces approximately 12 nm from the loop.

For TEM observations, it is important to know the mobility of loops at RT. The diffusivity at 300 K as predicted by the fitted  $E_{\rm mig}$  and  $D_0$  can be seen in figure 4. The diffusivity of vacancy loops is lower than that of interstitial loops, but with increasing N, they are getting closer to each other. The mobility of interstitial loops can be fitted by the  $N^{-1/2}$  law proposed for interstitial loops [19, 20]. No such dependency is observed for vacancy loops. A similar experimental dependence of the  $D_0$  prefactor on loop size in iron  $N^{-0.8}$  was reported by Arakawa *et al* [23]. Our prefactor  $D_0$  seems to follow the same  $N^{-0.81\pm0.29}$  for interstitial and vacancy loops if the results for a single vacancy and a single interstitial (N = 1) are omitted.

For comparison, we can at 300 K calculate the diffusivity  $D_{300\,\mathrm{K}}$  Total, including the phonon drag phenomenon, by not discarding the jumps larger than 1b. A comparison of  $D_{300\,\mathrm{K}}$  Arrh. and Total can be seen in figure 5. At 300 K the phonon drag phenomenon is significant only for SIA, while the dislocation loops are influenced much less.

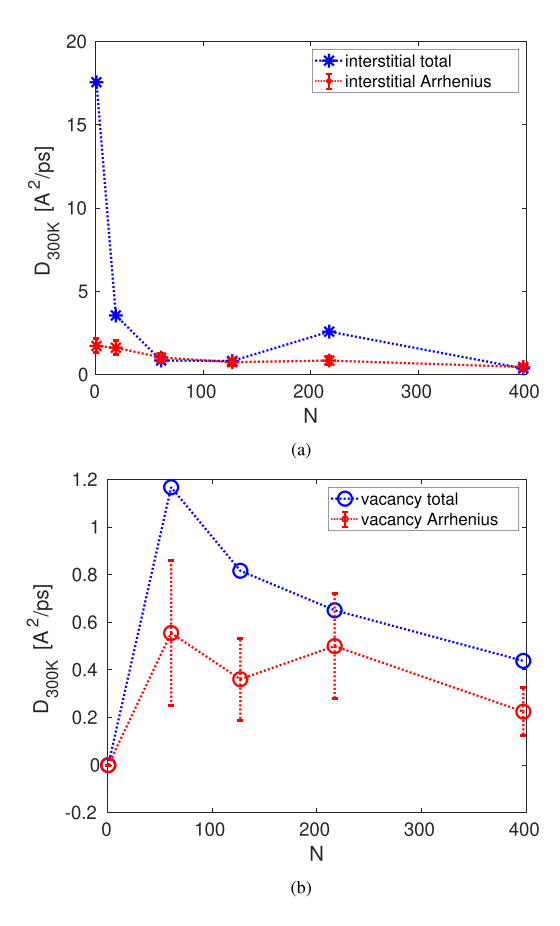


**Figure 5.** The thermally activated and total mobility, including the phonon drag phenomenon. (a) For interstitial loops and (b) for vacancy loops. The error bars in the thermally activated case correspond to standard deviations.

**Table 1.** The fitted parameters of thermally activated diffusion for interstitial loops and the predicted thermally activated and total diffusivity at 300 K, including the phonon drag phenomenon. The standard deviations of the fitted  $E_{\rm mig}$ ,  $D_0$ , and calculated  $D_{300\,\rm K}$  Arrh. are also indicated.

N	$E_{ m mig}$ (meV)	$\begin{array}{c} D_0 \\ (\mathring{A}^2  \mathrm{ps}^{-1}) \end{array}$	$D_{300\mathrm{K}}$ Arrh. $(\mathring{\mathrm{A}}^2\mathrm{ps}^{-1})$	$D_{300\mathrm{K}}$ Total (Å <sup>2</sup> ps <sup>-1</sup> )
1	$8.50 \pm 0.36$	$2.40 \pm 0.52$	$1.73 \pm 0.42$	17.52
19	$20.37 \pm 1.64$	$3.57 \pm 0.82$	$1.62 \pm 0.41$	3.56
61	$17.45 \pm 2.09$	$2.03 \pm 0.51$	$1.03 \pm 0.27$	0.86
127	$6.74 \pm 0.85$	$0.98 \pm 0.10$	$0.75 \pm 0.19$	0.82
217	$17.64 \pm 2.80$	$1.68 \pm 0.65$	$0.85 \pm 0.23$	2.59
397	$10.95 \pm 2.43$	$0.71 \pm 0.22$	$0.47 \pm 0.12$	0.38

The fitted thermally activated parameters  $E_{\rm mig}$  and  $D_0$  together with  $D_{300\,\rm K}$  Arrh. and  $D_{300\,\rm K}$  Total are reported in tables 1 and 3. Note that  $D_{300\,\rm K}$  Arrh. are obtained from fitted  $E_{\rm mig}$  and  $D_0$ , while  $D_{300\,\rm K}$  Total is a result of a single MSD simulation at 300 K.

**Table 2.** Parameters of thermally activated diffusion for interstitial loops from [21] for comparison.

N	E <sub>mig</sub> (meV)	$\begin{array}{c} D_0 \\ (\mathring{A}^2  \mathrm{ps}^{-1}) \end{array}$
1	44	10.4
7	26	4.7
19	31	4.0
37	30	3.2
61	25	2.2
85	29	2.0

**Table 3.** The fitted parameters of thermally activated diffusion for vacancy loops and the predicted thermally activated and total diffusivity at 300 K, including the phonon drag phenomenon. The standard deviations of the fitted  $E_{\rm mig}$ ,  $D_0$ , and calculated  $D_{300\,\rm K}$  Arrh. are also indicated.

N	E <sub>mig</sub> (meV)	$\begin{array}{c} D_0 \\ (\mathring{A}^2  \mathrm{ps}^{-1}) \end{array}$	$D_{300\mathrm{K}}$ Arrh. $(\mathring{\mathrm{A}}^2\mathrm{ps}^{-1})$	$D_{300 \mathrm{K}}$ Total $(\mathring{\mathrm{A}}^2 \mathrm{ps}^{-1})$
1	$1050 \pm 60$	$19.8 \pm 7.56$	0	0
19	_	_	_	_
61	$88.90 \pm 8.52$	$17.3 \pm 9.03$	$0.55 \pm 0.31$	1.17
127	$44.89 \pm 4.69$	$2.05 \pm 0.62$	$0.36 \pm 0.17$	0.82
217	$10.94 \pm 1.21$	$0.76 \pm 0.12$	$0.50 \pm 0.22$	0.65
397	$14.37 \pm 1.52$	$0.39 \pm 0.08$	$0.22 \pm 0.10$	0.44

# 4. Conclusions

We have investigated the diffusivity of the hexagonal vacancy and interstitial  $^{1}/_{2}\langle 1\,1\,1\rangle$  loops by MSD and developed a method to eliminate the influence of the phonon drag phenomenon at high temperatures, which is sometimes referred to as correlated diffusion. Our specific conclusions are the following:

- The mobility of small vacancy loops is lower than that of the corresponding interstitial loops.
   At larger sizes, the mobility becomes comparable, and perfect dislocation loops 'forget' their point defect nature.
- The migration barrier decreases with size for vacancy loops, while it remains low and almost constant for interstitial loops.
- The diffusivity of interstitial loops follows the  $N^{-1/2}$  law; this is not true for vacancy loops.
- At RT, the phonon drag phenomenon increases the SIA diffusion by nearly ten times, while the vacancy and interstitial loops diffusion is less affected.
- At higher temperatures, the phonon drag must be considered for both SIA and dislocation loop diffusion. In general, phonon drag should be accounted for in all high-temperature diffusion scenarios with low migration barriers.
- The 19 vacancy <sup>1</sup>/<sub>2</sub>(111) loop does not move; instead, it transforms at 800 K to energetically
  more favorable 19 vacancy void. A similar transformation likely occurs at high temperatures
  for all vacancy loops with diameters below 65 nm.
- Our method enables the accurate calculation of thermal activation parameters from correlated diffusion by effectively subtracting the phonon drag phenomenon.

#### Data availability statement

The data cannot be made publicly available upon publication because no suitable repository exists for hosting data in this field of study. The data that support the findings of this study are available upon reasonable request from the authors.

## **Acknowledgments**

Computational resources were provided by the e-INFRA CZ Project (ID: 90254), supported by the Ministry of Education, Youth and Sports of the Czech Republic. This work has been carried out within the framework of the EUROfusion Consortium, funded by the European Union via the Euratom Research and Training Programme (Grant Agreement No. 101052200—EUROfusion) and from the EPSRC (Grant Number EP/W006839/1). Views and opinions expressed are, however, those of the author(s) only and do not necessarily reflect those of the European Union or the European Commission. Neither the European Union nor the European Commission can be held responsible for them.

#### **ORCID iDs**

Jan Fikar © 0000-0003-1499-3958 Robin Schäublin © 0000-0002-8379-9705 Daniel R Mason © 0000-0002-1536-6254 Duc Nguyen-Manh © 0000-0001-6061-9946

#### References

- [1] Yi X, Sand A E, Mason D R, Kirk M A, Roberts S G, Nordlund K and Dudarev S L 2015 Europhys. Lett. 110 36001
- [2] Mason D R, Sand A E, Yi X and Dudarev S L 2017 Acta Mater. 144 905-17
- [3] Sand A E, Dudarev S L and Nordlund K 2013 Europhys. Lett. 103 46003
- [4] Sand A E, Mason D R, Backer A D, Yi X, Dudarev S L and Nordlund K 2017 Mater. Res. Lett. 5 357-63
- [5] Mason D R, Yi X, Kirk M A and Dudarev S L 2014 J. Phys.: Condens. Matter 26 375701
- [6] Ferroni F, Yi X, Arakawa K, Fitzgerald S P, Edmondson P D and Roberts S G 2015 Acta Mater. 90 380–93
- [7] Fikar J, Gröger R and Schäublin R 2017 Nucl. Instrum. Methods Phys. Res. B 393 186-9
- [8] Jónsson H, Mills G and Jacobsen K W 1998 Classical and Quantum Dynamics in Condensed Phase Simulations (World Scientific)
- [9] Swinburne T D and Dudarev S L 2015 Phys. Rev. B 92 134302
- [10] Swinburne T D, Ma P-W and Dudarev S L 2017 New J. Phys. 19 073024
- [11] Zhou W, Li Y, Huang L, Zeng Z and Ju X 2013 J. Nucl. Mater. 437 438-44
- [12] Fikar J, Schäublin R, Mason D R and Nguyen-Manh D 2018 Nucl. Mater. Energy 16 60–65
- [13] Fikar J and Schäublin R 2009 Nucl. Instrum. Methods Phys. Res. B 267 3218–22
- [14] Plimpton S 1995 J. Comput. Phys. 117 1–19
- [15] Mason D R, Nguyen-Manh D and Becquart C S 2017 J. Phys.: Condens. Matter 29 505501
- [16] Ackland G J and Thetford R 1987 Phil. Mag. A 56 15–30
- [17] Meyer W and Neldel H 1937 Z. Tech. Phys. 12 588
- [18] Yelon A, Movaghar B and Branz H M 1992 Phys. Rev. B 46 12244–50
- [19] Becquart C, Domain C, Sarkar U, DeBacker A and Hou M 2010 J. Nucl. Mater. 403 75-88
- [20] Derlet P M, Gilbert M R and Dudarev S L 2011 Phys. Rev. B 84 134109
- [21] Chen Y, Fang J, Liu L, Hu W, Jiang C, Gao N, Zhou H-B, Lu G-H, Gao F and Deng H 2019 J. Nucl. Mater. 522 200–11
- [22] Fang J, Liu L, Gao N, Hu W, Gao F and Deng H 2020 J. Appl. Phys. 128 065103
- [23] Arakawa K, Ono K, Isshiki M, Mimura K, Uchikoshi M and Mori H 2007 *Science* 318 956–9